2023 IEEE Symposium on Electromagnetic Compatibility & Signal/Power Integrity (EMC+SIPI) | 979-8-3503-0976-8/23/$31.00 ©2023 IEEE | DOI: 10.1109/EMCSIPI50001.2023.10241745

Static I-V based PIM Evaluation for Spring and Fabric-over-Foam Contacts

Kalkidan W. Anjajo[#1], Yang Xu[#2], Shengxuan Xia[#3], Yuchu He[*4], Haicheng Zhou[*5], Hanfeng Wang[*6], Jonghyun Park[♦7], and Chulsoon Hwang[#8]
[#]EMC Laboratory, Missouri University of Science and Technology, Rolla, MO, USA
[*]Google LLC, Mountain View, CA, USA
[♦]Mechanical and Aerospace Engineering, Missouri University of Science and Technology, Rolla, MO, USA
[1]kah5w@mst.edu, [8]hwangc@mst.edu

***Abstract*—Spring clips and fabric-over-foams (FOFs) are widely used in mobile devices for electrical connection purposes. However, the imperfect metallic connections tend to induce passive intermodulation (PIM), resulting in a receiver sensitivity degradation, known as RF desensitization. Due to the complexity of the PIM characterization, there is not yet a way to evaluate PIM performance using a simple setup for environments like factories. In this paper, a current-voltage (I-V) behavior-based PIM evaluation method is proposed and validated with various metallic contacts and contact forces. The test results demonstrated the feasibility of the PIM performance evaluation based on the measured static I-V curve.**

Keywords—passive intermodulation (PIM), radio frequency interference (RFI), fabric-over-foam, spring contacts, I-V curve

I. Introduction

In mobile devices, the degradation of receiver sensitivity (desensitization) is a significant concern. One of the causes is passive intermodulation (PIM). PIM is challenging to identify, as there are many causes – nonlinear materials, poor metallic contacts, surface oxidation, vibration, etc. [1]. Moreover, the generation mechanisms are complicated–semiconductor, electron-tunneling, electro-thermal, micro discharge, and contact mechanisms [2].

PIM in mobile applications is commonly caused by loose metal contacts. Among the contributing factors to PIM, the corresponding contact level is dominant [2], which models the metallic contacts as a metal-insulator-metal structure with current-dependent nonlinearity. This current-dependent nonlinearity can be modeled as a nonlinear resistor [3]. It has been observed that the PIM can be predicted based on the current voltage (I-V) characteristics of metallic contacts, the study in [4] achieved a good correlation between measured and theoretically calculated PIM under different bias voltages, based on the measured I-V curve of a silicon slice. A truncated current-distortion-based PIM modeling approach was successfully applied in [5], [6] on coaxial connectors. The work in [7] describes coaxial connectors' PIM behavior with the hyperbolic-tangent-based I-V curve. Moreover, nonlinear mathematical I-V models could reasonably predict the PIM of N-type coaxial connectors [8], [9]. Nevertheless, the above work only shows several cases, mostly limited to coaxial connectors, similar limitations are also observed regarding other PIM studies.

This work was supported in part by Google LLC and the National Science Foundation (NSF) under Grant No. IIP-1916535.

Presently, the spring clips and fabric-over-foams (FOFs) provide a good solution allowing number of modules to be assembled in a compact device. At the same time, the spring and FOF contacts tend to cause PIM because the contact junction is not soldered, resulting in RF desensitization if installed with insufficient contact force [10]. To characterize the PIM, expensive instruments and microwave devices are needed, such as s signal generator, duplexer, and spectrum analyzer, but usually these instruments are unavailable and inappropriate for large-scale testing in a factory setting. The ability to quantify PIM level in a factory setting would help reduce risk of RF desensitization caused by poor metallic contacts. In [11], a low cost 4 wire DCR measurement was proposed to estimate the contact generated PIM for spring contacts. However, the drawback for this method was, only the lowest PIM can be estimated but not the level of the PIM itself for each corresponding contact. Therefore, a simple setup to identify PIM risk at each contact is in demand.

In this paper, an estimation method to evaluate the third order PIM level of metallic contacts such as springs and FOFs from a polynomial fit of a current swept I-V curve at different contact forces is proposed. The third order coefficients of different contact cases are extracted and used in the circuit model as figures of merit.

II. Measurement System and Procedures

A. Test Setup

A measurement system was built to investigate the correlation between the PIM and I-V, as shown in Fig. 1. The PIM level measurement setup was adapted from [10].

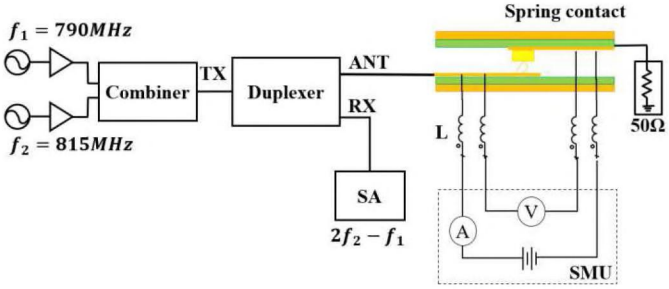

Fig. 1. PIM-IV measurement system.

The amplified signals (790 and 815 MHz) are combined and then transmitted to the transmitter port of a low-PIM duplexer - frequency range: 790~821 MHz (Transmitter) and 832~863 MHz (Receiver). At the antenna port of the duplexer, the combined two-tone signal is injected to the DUT – the spring contact or FOF contact. The other end of the DUT is terminated with a high-power and low-PIM 50 Ω load. Only the third order PIM (the highest magnitude compared to other higher order intermodulation products) has been considered and only $2f_2 - f_1$, $(f_2 > f_1)$ is monitored. The induced third order PIM (840MHz) is monitored by the spectrum analyzer (SA), with 10 Hz resolution bandwidth. A 4-wire resistance measurement setup was implemented to allow accurate static I-V tests with a source measure unit (Keithley 2401). Surface mount inductors were placed to prevent the impact on the RF signal path while conducting I-V tests.

The detailed view of the test fixture for the spring contact is shown in Fig. 2(a), the spring clip is soldered on the bottom board, and a piece cut out from an actual phone chassis namely (landing pad) is soldered on the top board. The top board is connected to a force gauge with 0.001N resolution. The top board's height is controlled by a step motor of 0.3 μm resolution. According to the S11 and S21 performance [10], by pressing down the top board until there is a good contact, the capacitive coupling between the two boards provides a good enough return path.

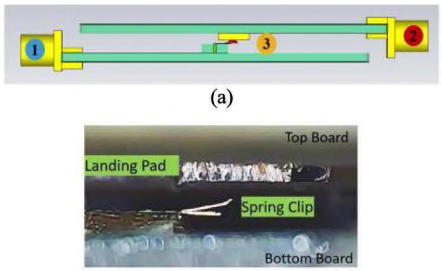

(a)

(b)

Fig. 2. Test fixture for spring contact: (a) full-wave simulation model, (b) spring contact – spring clip and landing pad.

B. I-V Test Procedures

The signal generators are turned off to disable the PIM measurement, and current is then swept from 10 mA to 150 mA, for both polarities' currents: +10, -10, +16, -16, +22, -22, …, +150, -150 mA as shown in Fig. 3. Gradually increasing the current amplitude helps to avoid potential high current melting at the tiny contact junction in the beginning.

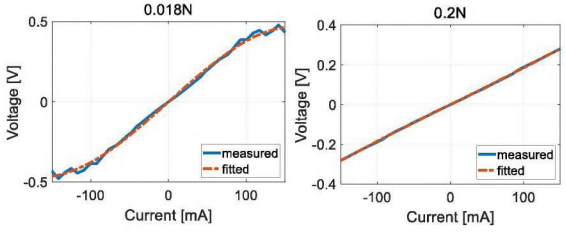

(a) (b)

Fig. 3. I-V test results: (a) I-V curve at loose contact, (b) I-V curve at good contact.

If the negative sweep is processed after finishing the positive sweep, the PIM level may change dramatically.

The highest input power used for this work is 20 dBm, while the spring contact resistance is typically several Ohms or lower, and the source and load impedance is 100 Ω in total, so the maximum current is set to be 150 mA. As the input power increases, the current needed likewise increases. For example, if measured to a higher input power such as 30 dBm, then the maximum current needs to be 400 mA. During the measurement of the DC resistance by sweeping the current, the I-V curve of each contact case could be generated. From Fig. 4(a), it can be clearly observed in the measured I-V curves that the curves are more non-linear with lower contact force, i.e., loose contact case, and becomes more linear as the contact force increases. Fig. 4(b) shows the corresponding PIM levels for different contact forces. From the correlation, it can be concluded that the nonlinear coefficient extracted from the I-V curve can be used to represent and characterize the PIM level.

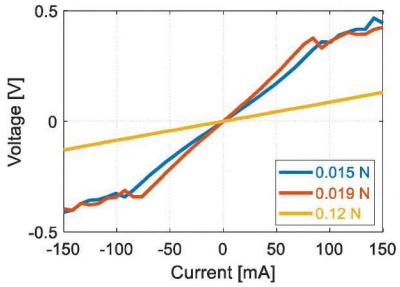

(a)

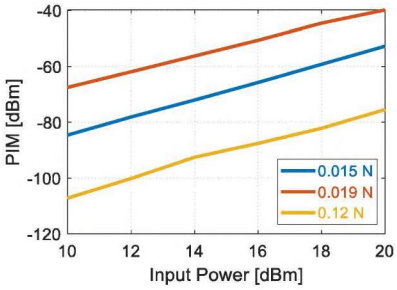

(b)

Fig. 4. Measurement results for spring clip and chassis landing pad contact under different contact forces: (a) I-V curve, (b) PIM versus input power.

The measured I-V curve is then fitted with a third order polynomial and the polynomial coefficients are extracted. The third order coefficient, a_3, will be used later in this paper to estimate the PIM level at each corresponding contact case.

$$V = a_0 + a_1 I + a_2 I^2 + a_3 I^3 \qquad (1)$$

The PIM levels can be checked before and after the I-V tests to ensure that the contact condition has not been changed. Reasonable small differences between pre- and post-PIM the contact junction remains unchanged. It was observed that the I-V sweep can dramatically change the PIM behavior for some loose (slight) contacts and the discrepancy between pre- and post-PIM was above 10dB. To ensure the measured I-V curve

represents the PIM behavior, only the datasets within 5dB discrepancy between pre- and post-PIM were collected in this paper to demonstrate the relationship between the I-V behavior and the PIM level. Repeatability test for multiple samples were taken before making conclusions on the results.

C. PIM Estimation

A simplified circuit model of the test fixture with a nonlinear resistor and a 50-ohm load is depicted in Fig. 5. A nonlinear resistor representing the fitted I-V curve based on (1), is represented as DUT. The PIM level can be estimated based on the V_{f3} (voltage at the PIM frequency which equals $2f_2 - f_1$).

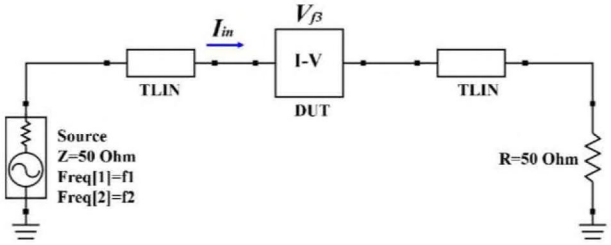

Fig. 5. Schematics of the nonlinearity representation.

The input current of the I-V block can be expressed as

$$I_{in} = I_{1_{in}} \cdot cos\omega_1 t + I_{2_{in}} \cdot cos\omega_2 t, \quad (2)$$

Then (1) can be represented as

$$V = a_0 + \sum_{n=1}^{3} (a_n {I_{in}}^n). \quad (3)$$

The third order PIM component can be extracted (4) and the current can be solved by the cubic equation (5) as follows.

$$V_{f3} = a_3 \frac{3}{4} I_1 I_2^2 \, cos(2\omega_2 - \omega_1)\, t \quad (4)$$

$$a_3 I^3 + a_2 I^2 + (a_1 + Z_s + Z_L) I + (a_0 - V_s) = 0 \quad (5)$$

where Z_S is the 50 Ω source impedance, Z_L is the 50 Ω load, and V_S is the source voltage. Finally, the PIM_3 can be calculated from the power at V_{f3} and can be expressed as

$$PIM_3[dBm] = 20 \cdot log \left| a_3 \frac{3}{4} I_1 I_2^2 \right| + 13.01 \quad (6)$$

The analytic expression of the PIM is verified by comparing the mathematical calculation with the circuit simulation. Based on (6), the relationship between the PIM and the third order coefficient a_3 can be extracted as

$$PIM_3 \propto log_{10}|a_3|. \quad (7)$$

An assumption can be made as (8), because the source and load impedance are much higher than the spring contact resistance. As a result, the PIM is only related to the third order coefficient.

$$I_{in1} = I_{in2} \cong \frac{V_s}{2(Z_L + Z_s)} \quad (8)$$

The test fixture's impact is further considered in the estimation process, as shown in Fig. 6. The 3-port S-parameter block was extracted from the full-wave simulation in representing the test fixture. While this approach can better represent the actual setup, it was found that the simulation results are close enough to the numerical calculation – within 1.5dB. Therefore, the numerical approach (6) is applied in the following estimation process for implementation. The PIM performance of spring and FOF contacts are predicted and compared to measured results in this section.

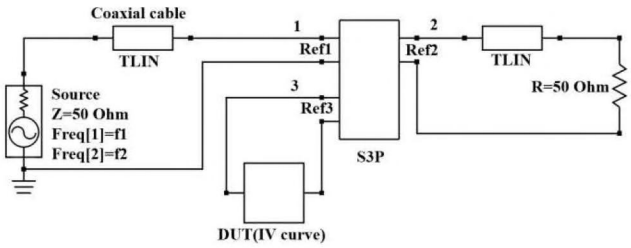

Fig. 6. PIM estimation circuit schematics including the setup impact.

III. Measurement Validation

A. Spring Contacts

In this study, three spring clips shown in Fig. 7 are used to verify the PIM estimation process. The bottom part of the spring clip is soldered to the bottom PCBs' trace and the curved tip structure on the other end of the spring, contacts the landing pad. The measurement and estimation results based on the spring-chassis contact are summarized in Fig. 8. Note that only the data at 20 dBm input power are shown. Nevertheless, it adequately represents the simulation performance with 10-20 dBm input power because the measured and simulated PIM follow a 3 dB / dB regrowth rate as shown Fig. 4(b).

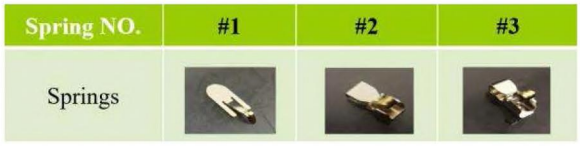

Fig. 7. Three types of spring clip characterized.

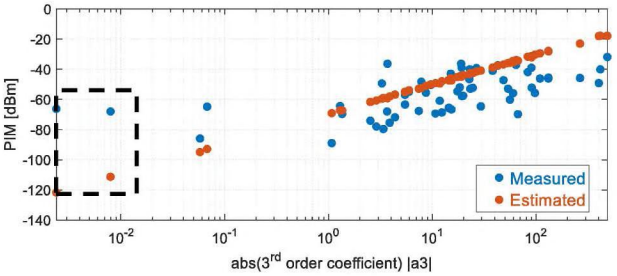

Fig. 8. Measured and simulated PIM (at 20 dBm input power) versus third order coefficient (a3) from the fitted I-V curve.

The data points that occurred in the high-PIM region (>−60dBm) are due to lose spring contact, which corresponds to stronger nonlinearity. The large discrepancy of the two cases marked in the dashed black block is caused by the self-contact effect [12]. There is already a considerable amount of contact

force when the self- contact is made, so the measured I-V curve is much more linear (i.e., the estimated PIM level will be small). On the other hand, the self-contact induces high PIM. As a result, the PIM is much underestimated since the I-V measurement only reveals the main body of the spring clip (of low impedance) instead of the self-contact region. Overall, the simulation captures the trend: the PIM is proportional to the $\log_{10}|a_3|$.

The discrepancy between estimated and measured PIM is summarized in Fig. 9. There are 120 cases in each group, and for each group, the measured and estimated PIM level is compared with 10-20 dBm input power. More than 96% of cases are captured within 20 dB when compared to measurements.

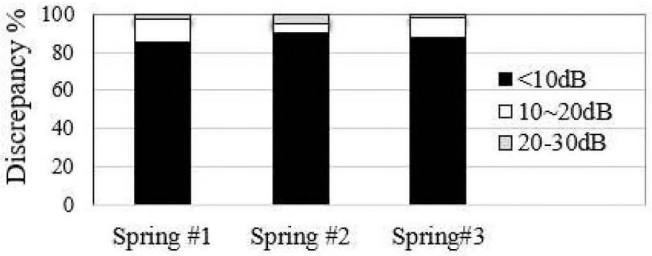

Fig. 9. Discrepancy of measured and simulated PIM for etched chassis and spring clips.

B. FOF Contacts

Four types of FOFs shown in Fig. 10, are tested. The test setup is similar to Fig. 1. The only difference is that the spring clip is changed to FOF. The measured and simulated PIM for FOF at 20 dBm input power is shown in Fig. 11(a); The PIM is proportional to $log_{10}|a_3|$, as mentioned earlier. In addition, from Fig. 11(b), notice that the PIM level does not always decrease with higher contact force, while the I-V based estimation can still reasonably capture the trend, primarily within 10 dB discrepancy. More than 500 cases were collected with different FOF types and contact forces, and the input power is swept among 10-20 dBm for each case. Fig. 12 summarizes the discrepancy between the measurement and estimation. Ninety percent of the cases from woven-type FOF are captured within 10 dB discrepancy.

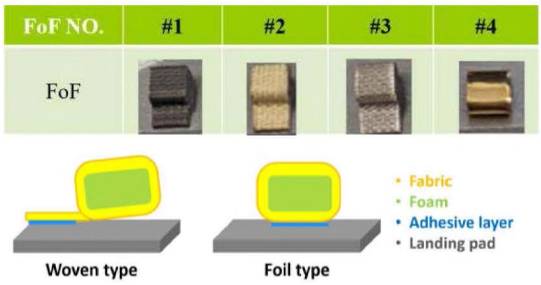

Fig. 10. Different types of FOF: The electrically conductive-plated fabric is wrapped over a foam, the adhesive layer on the bottom is used for installment purposes.

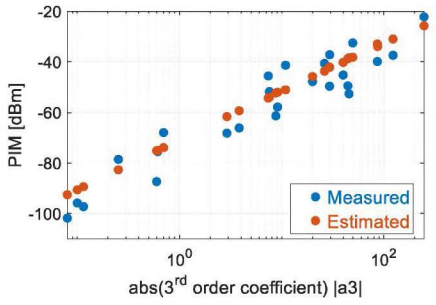

(a)

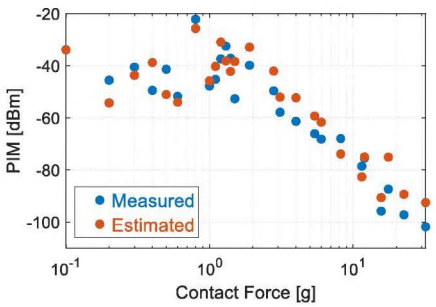

(b)

Fig. 11. Measured versus estimated PIM for FOF #4 at 20 dBm input power: (a) PIM versus third order coefficient from the fitted I-V curve, (b) PIM at various contact forces.

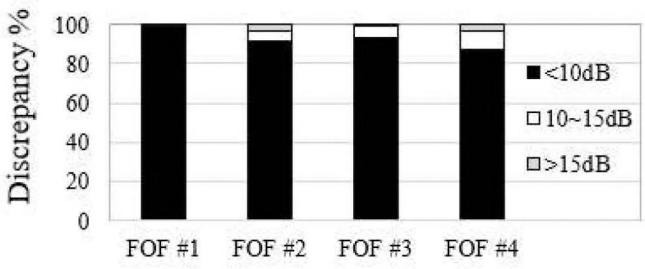

Fig. 12. Discrepancy of measured and simulated PIM for various combinations of landing pad and FOF.

C. Discussion

Several causes account for the discrepancies. First, the tiny contact area of spring contact, especially at loose contact force, makes it challenging to achieve an accurate PIM prediction. The smaller the contact area, the higher the nonlinear current density for a certain PIM level, resulting in unstable mechanical connection. Therefore, statistical analysis based on a large database is needed. Second, the imperfect I-V test – the current path of the static I-V test may be different from the RF current path. The pulsed I-V tests have potential to overcome the issue. Third, the I-V test itself may change the characteristics of the metallic contact, which is why the pre- and post-PIM need to be monitored to make sure the measured I-V can be correlated with the PIM. Besides, only the third order polynomial is applied for the I-V fitting, so numerical error exists. Though higher-order polynomial fit allows a better fitting, it increases the possibility to cause overfitting.

IV. Conclusion

An I-V based PIM estimation method is proposed to estimate the PIM in spring and FOF contacts. The overall discrepancy of PIM between measurement and I-V based estimation is within 20 dB in 85% cases of spring contacts and within 10 dB in 90% cases of FOF contacts. It was observed that the higher nonlinearity of I-V shows, the higher the PIM levels are observed. Considering the complexity and expensive cost of PIM setup, a simple way to identify the possible high PIM risk is needed. The I-V test provides the way with easier implementation in massive factory tests. Correspondingly, the spring clip and FOF suppliers can have a simpler and inexpensive way to try various combinations of material, surface treatment, and product shape to optimize the design.

V. References

[1] P. L. Lui, "Passive intermodulation interference in communication systems," *Electronics and Communication Engineering Journal*, vol. 2, no. 3, p. 109, June 1990

[2] P.-L. Lui, "A Study of Intermodulation Interference Due to Non-linearities in Metallic Structures," Ph.D dissertation at the University of Kent, Canterbury p. 215, 1990.

[3] J. J. Henrie, A. J. Christianson, and W. J. Chappell, "Linear–Nonlinear Interaction and Passive Intermodulation Distortion," *in IEEE Transactions Microwave Theory and Tech*niques, vol. 58, no. 5, pp. 1230–1237, May 2010.

[4] X. Zhao *et al.*, "Analytic Passive Intermodulation Model for Flange Connection Based on Metallic Contact Nonlinearity Approximation," *in IEEE Transactions Microwave Theory and Tech*niques, vol. 65, no. 7, pp. 2279–2287, Jul. 2017.

[5] Q. Jin, J. Gao, G. T. Flowers, Y. Wu, and H. Huang, "Passive Intermodulation Models of Current Distortion in Electrical Contact Points," *IEEE Microwave and Wireless Components Letters*, vol. 29, no. 3, pp. 180–182, Mar. 2019.

[6] Q. Jin, J. Gao, L. Bi, and Y. Zhou, "The Impact of Contact Pressure on Passive Intermodulation in Coaxial Connectors," *in IEEE Microwave and Wireless. Components Letters*, vol. 30, no. 2, pp. 177–180, Feb. 2020.

[7] J. Henrie, A. Christianson, and W. J. Chappell, "Prediction of Passive Intermodulation from Coaxial Connectors in Microwave Networks," *in IEEE Transactions Microwave Theory and Tech*niques., vol. 56, no. 1, pp. 209–216, Jan. 2008.

[8] Q. Jin, J. Gao, G. Xie, G. T. Flowers, and R. Ji, "A study of the passive intermodulation induced by nonlinear characteristics of RF connectors," *in 2016 IEEE 62nd Holm Conference on Electrical Contacts (Holm)*, Oct. 2016, pp. 1–8.

[9] A. J. Christianson, J. J. Henrie, and W. J. Chappell, "Higher Order Intermodulation Product Measurement of Passive Components," *in IEEE Transactions Microwave Theory and Tech*niques, vol. 56, no. 7, pp. 1729–1736, Jul. 2008.

[10] S. Xia et al., "Practical Fixture Design for Passive Intermodulation Tests for Flexible Metallic Contacts," *in 2022 IEEE International Symposium on Electromagnetic Compatibility & Signal/Power Integrity (EMCSI)*, 2022, pp. 17-22.

[11] S. Xia et al., "*Gassian Process Regression Analysis of Passive Intermodulation Level and DCR for Spring Contacts*," 2021 IEEE International Joint EMC/SI/PI and EMC Europe Symposium, Raleigh, NC, USA, 2021, pp. 935-939

[12] J. Li et al., "Self-contact Introduced Passive Intermodulation Characterizations for Captured Springs," *in IEEE International Joint EMC/SI/PI and EMC Europe Symposium*, Raleigh, NC, USA, 2021, pp. 929-934.